1 Predicting Pore Volume, Compressive Strength, Pore Connectivity,

and Formation Factor in Cementitious Pastes Containing Fly Ash

- 2
- 4 **Authors:** Keshav Bharadwaj ^a, Rita Maria Ghantous ^a, Feyza Sahan ^b, O. Burkan Isgor ^a, and
- 5 W. Jason Weiss ^{a*}
- ^a School of Civil and Construction Engineering, Oregon State University, Corvallis OR, 97331,
- 7 USA
- 8 ^b Civil Engineering Department, Ozyegin University, Istanbul, Turkey
- 9 * Corresponding Author; e-mail: jason.weiss@oregonstate.edu; postal address: 101 Kearney
- Hall, 1491 SW Campus Way, Corvallis, OR 97331

11

- 12 **Keywords:** cement paste, fly ash, compressive strength, porosity, formation factor,
- 13 thermodynamic modeling.

14 Abstract:

- 15 This paper describes the use of thermodynamic modeling to predict the reaction products and
- properties of cementitious pastes containing fly ash. A pore partitioning model is used to
- estimate the gel and capillary pore volumes. The paste performance is predicted in terms of its
- porosity, compressive strength, formation factor, and deicing salt damage susceptibility. A
- 19 model is proposed to quantify the pore refinement that occurs when fly ash is used.
- 20 Comparisons are made between the predicted properties by the model and properties of
- 21 experimentally measured cementitious pastes with two fly ashes at different water-to-binding
- 22 ratios and varying replacement levels. The error in predicting porosity is 5%; compressive
- 23 strength is 14% for OPC systems and 26% for OPC+FA systems; and formation factor is
- between 1-20% for OPC systems, 13-26% for the OPC+20%FA systems, and 18-46% for the
- OPC+40%FA systems.

26

1 INTRODUCTION

A variety of empirical or quasi-theoretical approaches exist to predict the compressive strength of concrete [1-3]. These models typically use the water-to-binder ratio (*w/b*) as a surrogate for total porosity to estimate strength [4]; however, they typically do not explicitly consider the pore size distribution. This approximation is often limited to systems made with Ordinary Portland Cement (OPC). Several strength models have been proposed to account for the use of Supplementary Cementitious Materials (SCMs) in concrete. However, the SCM models often rely on empirical fitting to determine the extent of SCM reactions [5, 6], or use "activity factors" [7-10] and "efficiency factors" (also called "k-factors") that are used to convert the mass of an SCM to an equivalent mass of OPC [11]. These approximations require experimental calibration for each SCM binder chemistry and reactivity, and may not yield accurate predictions of performance related properties (e.g., compressive strength) for most concrete mixtures. Further, they do not allow for determining other critical concrete properties such as porosity, electrical resistivity, formation factor, or time to critical saturation.

Quasi-theoretical models, such as the one developed by Powers and Brownyard (henceforth call the "PB" model), can predict the volume fractions of different types of pores (e.g., gel pores, capillary pores, pores due to chemical shrinkage) as a function of the degree of hydration [12, 13]. Powers and Brownyard also used porosity predictions of their model to predict compressive strength using the gel-to-space ratio that can be obtained from the porosity calculations [12]. While initially developed for OPC systems, others have sought to extend this approach to systems containing SCMs such as silica fume [14] and fly ash [15], however, this is not straightforward as the chemical composition and reactivity of SCMs show a large degree of variability [16, 17].

Advancements in computational resources have also resulted in predictive modeling tools to compute the porosity of cementitious systems using numerical modeling techniques that are built on theoretical bottom-up (micron-scale to millimeter/centimeter scale) algorithms. Such models include CEMHYD3D [18, 19], HYMOSTRUC [20, 21], DuCOM [22-24], and µic [25, 26]. Many of these models predict the total porosity of cementitious systems on a small scale, but they often do not consider the wide range of SCM chemistries and reactivities, hence, also rely on empirical calibration.

52

53

54

55

56

57

58

59

60

61

62

63

64

65

66

67

68

69

70

71

72

73

74

75

76

Thermodynamic modeling has also been used to predict the reaction products of hydration in cementitious systems [27-29]. Azad et al. [30] developed the Pore Partitioning Model (PPM) that could be used to estimate the volumes of gel pores and capillary pores for OPC-based pastes. Glosser et al. [31] extended the PPM to include SCMs. Bharadwaj et al. [32] upscaled the PPM to concrete and developed the Pore Partitioning Model for Concrete (PPMC) [32]. The general framework of the PPMC is shown in Figure 1. The inputs to the model are the mixture proportions of the concrete (amounts of air, water, OPC, SCM), physical properties of the binder (specific gravity and fineness of the OPC and SCM(s) used), the chemical composition of the binder (OPC and SCM(s) used), and the maximum degree of reactivity of the SCM (DOR*), which is the amount of SCM that is available to react [16]. The model has the potential to predict several key performance parameters of concrete, such as the calcium hydroxide (CH) content, porosity, compressive strength, formation factor, and time to critical saturation. Previously, the PPMC model has been used to predict the porosity, formation factor, and time to critical saturation of concrete made with OPC [32]; however, there is a need for a comprehensive experimental study does to validate the predictions of the models for OPC+SCM systems. In addition, this work provides the predictions of CH, porosity, compressive strength, and formation factor using the PPMC model. The model results are compared to experimental data. Furthermore, it was assumed in the PPMC model that the

microstructures of OPC- and OPC+SCM-based systems are similar, while it has been established that pore refinement occurs in OPC+SCM systems [33-36]. Therefore, the limitations of these models with respect to their ability to consider pore refinement need to be examined experimentally.

In this work, we compare the predictions of the PPM and PPMC frameworks to experimental data to explore the limitations of the models. Further, an empirical model is proposed to quantify the pore refinement by incorporating the consumption of CH due to the pozzolanic reactions of SCMs. The work involves tests that have been performed on systems containing OPC and OPC + fly ash at different w/b and fly ash replacement levels. Several performance parameters are examined using both experimental and theoretical approaches. These performance parameters include porosity, CH content, formation factor (before and after capturing the pore refinement), and the compressive strength.

The PPMC Framework

Inputs

- w/b
- SCM Replacement
- OPC & SCM composition
- SCM reactivity
- Alkali release factor
- Volume of entrained and entrapped air
- Aggregate volume & properties

Outputs of PPM

- Unhydrated Cement
- · Gel Solids
- · Gel Water
- Capillary Water
- Chemical Shrinkage
- Pore Solution Composition and Resistivity

Outputs of PPMC

- Porosity
- Matrix saturation
- Critical Saturation, and time to critical saturation
- · Formation Factor
- Compressive Strength
- Transport Properties

Figure 1. Outline of the PPMC, showing the inputs to the model, the outputs of the PPM, and the predictions of the PPMC (PPM scaled to concrete). Performance parameters such as porosity, formation factor (and its relation to transport), and compressive strength are explained in future sections. Information on other performance parameters can be found in reference [32].

89

90

91

92

77

78

79

80

81

82

83

84

85

86

87

2 MODELING APPROACH

2.1 Thermodynamic Calculations

In this work, thermodynamic modeling of cementitious systems is performed using the GEMS3K [37, 38] software coupled with the CEMDATA database [39-41]. GEMS3K performs thermodynamic modeling by determining the phase assemblage of a cementitious system that minimizes its Gibbs Free Energy. The GEMS/CEMDATA framework can be used to calculate the molar amounts of solid, aqueous, and gaseous products of reactions and the activities of ions in the pore solutions at thermodynamic equilibrium. This framework has been used to obtain the phase assemblage and pore solution composition of OPC systems [28, 29], and OPC+SCM systems [42]. GEMS3K v3.5 was coupled with CEMDATA v18 [27] was used to predict the outputs of cementitious and pozzolanic reactions. The formation of some of the carbonate-ettringite, hydrotalcite, and hydrogarnet phases were blocked, based on evidence from the literature showing that these phases are frequently not observed to form in substantial quantities in cementitious systems at ambient temperatures (less than 60°C) [29, 40, 42, 43].

2.2 Kinetic Models

Thermodynamic modeling allows the calculation of the phases in a system at equilibrium conditions. However, in reality, cementitious systems are in a transient state at any given time. As such, kinetic models are used along with thermodynamic modeling to model cementitious systems in a transient state. In a previous study, the Parrot-Killoh (PK) model for OPC was modified (Modified Parrot-Killoh, MPK, model) for OPC + Fly Ash (OPC+FA) systems [44] with improved kinetic parameters to account for SCMs [45]. The MPK model predicts the masses of clinker phases in cement (C₃S, C₂S, C₃A, and C₄AF) and oxide phases in the fly ash (SiO₂, Al₂O₃, and CaO) that are available to react at a given age, i.e., the degree of reaction of the phase (*DOR_{ph}*). The inputs to the MPK model are the total mass of the clinker phases in the OPC, and the masses of amorphous SiO₂, Al₂O₃, and CaO in the fly ash [45]. The

amorphous masses of SiO₂, Al₂O₃, and CaO in the fly ash were determined using X-Ray Fluorescence and Quantitative X-Ray Diffraction [45]. The degree of reaction of the system (denoted by DOR_{sys}) is calculated as the mass normalized average of the degree of reaction of the clinker phases in the cement (C₃S, C₂S, C₃A, and C₄AF) and oxide phases in the fly ash (SiO₂, Al₂O₃, and CaO), shown in equation (1):

$$DOR_{sys} = \frac{\sum_{ph} DOR_{ph} \cdot m_{ph}}{\sum_{ph} m_{ph}} \tag{1}$$

where m_{ph} is the input mass of each phase in consideration. The DOR_{sys} is determined by matching the amount of non-evaporable water calculated using thermodynamic modeling to the non-evaporable water obtained from experiments. It should be noted that in a number of mixtures with large SCM replacements (and/or reactivities), pozzolanic reactions result in the full consumption of CH. It is possible that some CH remains inaccessible in the analysis timeframes of this work due to the formation of hydration products on the CH surface [46]; however, this was not considered in this work.

2.3 The Pore Partitioning Model (PPM)

Thermodynamic modeling, while powerful, indicates the total water present in cementitious systems (i.e., the total volume of pores). Thermodynamic modeling alone cannot quantify the spatial distribution of reacted products or distinguish the pore size or the volume of water in the various sized pores in cementitious systems. Recent work has shown that thermodynamic modeling can be synergistically combined with principles from the Powers-Brownyard model [12, 13, 47] to determine the amount of gel water and capillary water in OPC systems [30], and then be extended to OPC+SCM systems [31]. This approach is referred to as the "Pore Partitioning Model" (PPM) that has been developed in [30, 31]. The PPM can be used to determine the volume fraction of unhydrated binder (v_{ub}) , gel solids (v_{gs}) , gel water (v_{gw}) , capillary water (v_{cw}) , and chemical shrinkage (v_{cs}) in cementitious pastes.

2.4 Predicted properties

2.4.1 Calcium Hydroxide

Calcium hydroxide (CH) in concrete provides the buffer capacity in concrete to stabilize its pH, which has implications for corrosion of steel in concrete [48], alkali-silica reaction (ASR) [36, 49], and carbonation of concrete [50]. In recent years, it has been documented that the CH content of cementitious systems is directly related to the potential for calcium oxychloride (CaOxy) formation in concrete, which has been linked to damage when deicing salts are used [46, 51-54].

2.4.2 Porosity

Cementitious pastes are porous materials with pores occupying a wide range of sizes. The porosity of cementitious pastes is defined as the sum of all voids in the system. The cementitious pastes are considered to be composed of two components: (1) pores in the hydrated cement paste (gel pores, capillary pores, and pores due to chemical shrinkage), which can be represented volumetrically by V_{paste} , and (2) entrapped air voids, which can be represented volumetrically by V_{air} . Consider a unit volume of the system ($V_{paste} + V_{air} = 1$). The hydrated cementitious paste consists of other volumetric fractions: unhydrated binder (v_{ub}), gel solids (v_{gs}), gel water (v_{gw}), capillary water (v_{cw}), and pores due to chemical shrinkage (v_{cs}). As such, the porosity of the paste (ϕ_{paste}) can be calculated as the sum of the gel water, capillary pores, pores due to chemical shrinkage, and the air voids.

$$\phi_{paste} = V_{air} + (v_{gw} + v_{cw} + v_{cs}) \cdot V_{paste}$$
(2)

2.4.3 Compressive Strength

The compressive strength of cement paste is a critical parameter in predicting the mechanical response of a concrete structure. While there are many models available in the literature to calculate compressive strength [1-4], in this work, the compressive strength is

calculated using the concept of the gel-to-space ratio proposed by Powers and Brownyard [12].

The gel-to-space ratio (gsr) is defined as the ratio of the volume of hydrated cement gel in the

system (V_{gel}) to the space available for the gel to occupy in the system (V_{space}) :

$$gsr = \frac{V_{gel}}{V_{space}} = \frac{(v_{gw} + v_{gs})V_{paste}}{1 - v_{ub} \cdot V_{paste}} = \frac{(v_{gw} + v_{gs})V_{paste}}{V_{air} + (v_{gs} + v_{gw} + v_{cw} + v_{cs})V_{paste}}$$
(3)

Powers and Brownyard used a power law to relate the gel-space ratio to the strength of cement pastes (f'_c) as shown in equation (4) [12].

$$f_c' = a_1 (gsr)^{a_2} \tag{4}$$

where a_1 and a_2 are constants typically fit to experimental data.

The calculation of compressive strength using equations (3) and (4) relies on the evaluation of the coefficients in the model (a_1 and a_2). In this work, these coefficients are chosen to be $a_1 = 138$ MPa and $a_2 = 3$ by curve fitting to the strength of pastes [55]. The value of the exponent $a_2 = 3$ agrees well with Powers and Brownyard's work on OPC mortars [12], and lies in the range of values observed by [55]. Various values of a_1 have been determined by experimental work in literature, ranging from 110 MPa to 300 MPa [12, 56-59], and this is explained by Powers and Brownyard [12], who hypothesized that the value of a_1 depends on the intrinsic strength of the gel. As such, the values of the empirical constants $a_1 = 138$ MPa and $a_2 = 3$, are used in the rest of this work.

2.4.4 Formation Factor

The formation factor [60] of a porous system is a way to characterize its microstructure. The formation factor can be used as an indicator of its transport properties [61, 62]. Recent research has shown that the formation factor of concrete can be related to the rapid chloride permeability (RCPT) test [63], ionic diffusion coefficients [61, 64, 65], water permeability and secondary sorption [62, 66-68]. Therefore, the formation factor is an important property that

can be used to predict the durability in concrete [32, 69]. The formation factor of a cementitious paste is traditionally defined as the inverse product of bulk porosity (ϕ_{paste}) and pore connectivity within the paste (β_{paste}), as shown in equation (5) [66]:

$$F = \frac{1}{\phi_{paste} \cdot \beta_{paste}} \tag{5}$$

The formation factor can also be defined in terms of the electrical properties of the cementitious system, as the ratio of the resistivity of the bulk system (ρ_{bulk}) to the resistivity of the fluid filling the pores (ρ_{ps}) [60], as shown in equation (6):

$$F = \frac{\rho_{bulk}}{\rho_{ps}} \tag{6}$$

The formation factor of a saturated porous medium (such as cement paste) can be calculated using equation (5) or equation (6). The PPMC framework [32] is used to calculate the formation factor of the cementitious pastes chosen for the study by computing the porosity and the pore connectivity and using equation (5). Hydrated paste is assumed to consist of calcium silicate hydrate (C-S-H) and other hydration products as impermeable gel solids interspersed with pore solution occupying the gel and capillary pores. The pore connectivity of hydrated paste (β_{paste}) is assumed to be the summation of the pore connectivity of the gel and capillary pores, as shown in equation (7).

$$\beta_{paste} = \beta_{qel} + \beta_{cap} \tag{7}$$

where β_{gel} is the pore connectivity of the gel, and β_{cap} is considered to be the pore connectivity of the capillary phase. The formation factor of gel solids is considered to be constant at 400, based on evidence from literature [70-72]. The porosity of the gel (φ_{gel}) is computed using the pore partitioning model [30, 31], and this value typically ranges from 26-27% for OPC to 29-38% for OPC+FA systems, consistent with the literature [12, 13, 31]. The pore connectivity of

the gel can be determined using the definition of formation factor applied to the gel phase, as shown in equation (8).

$$\beta_{gel} = \frac{1}{F_{gel} \cdot \varphi_{gel}} = \frac{1}{400 \cdot \varphi_{gel}} \tag{8}$$

Following the approach of [32], the capillary pore connectivity (β_{cap}) may be determined using a model for pore connectivity proposed in [73], and shown in equation (9):

$$\beta_{cap} = \frac{1}{\left(1 + b_1 \cdot \frac{1 - \phi_{paste}}{\left(\phi_{paste} - \phi_{thres}\right)^{b_2}}\right)^2} \tag{9}$$

where ϕ_{paste} is the total porosity of hydrated cementitious paste, ϕ_{thres} is the percolation threshold of the medium, set to volume fraction of gel water (v_{gw}) , and b_1 and b_2 are dimensionless empirical constants determined from experiments. The values of b_1 and b_2 were calibrated to data from the literature for OPC cement pastes [74], OPC mortars [62], and OPC concretes [66] and nearly consistent values of $b_1 = 2.4$ and $b_2 = 0.85$ were obtained. As such, these values are used for the prediction of the pore connectivity of hydrated pastes. With the pore connectivity of the gel and capillary phases known from equations (8) and (9), respectively, the pore connectivity of the paste may be calculated using equation (9). Using information on the porosity from equation (4), the formation factor of the paste can be calculated using equation (5).

3 EXPERIMENTAL STUDY

An experimental program has been conducted to measure the non-evaporable water content, CH content, porosity, compressive strength, and, bulk resistivity (which was used to determine the formation factor) of cementitious pastes with different fly ash replacement and different fly ash reactivity.

3.1 Materials

Table 1 lists the chemical and physical properties of OPC (ASTM C150-19) and fly ash used in this study. The ultimate degree of reactivity (DOR*) of the fly ashes used in this study was determined based on the measured heat released and CH consumed using the test method developed in [16]. The ultimate degree of reactivity (DOR*) of Fly Ash 1 was found to be 52%, and the DOR* of Fly Ash 2 was found to be 23%.

Table 1. Chemical composition and physical properties of raw materials. Fly ash composition is determined using X-Ray fluorescence [75].

	Cement	Fly Ash 1	Fly Ash 2	
	Chemical composition (in weight %)			
SiO ₂	20.4	28.9	40.0	
CaO	63.2	27.3	21.2	
Al ₂ O ₃	4.7	14.8	16.8	
Fe ₂ O ₃	3.3	4.7	6.2	
MgO	2.5	3.8	4.3	
SO ₃	2.8	11.9	0.8	
Na ₂ O _{eq}	0.54	0.94	1.4	
Limestone	3	-	-	
(87% CaCO ₃)				
Loss on	1.4	3.2	1.1	
ignition (LOI)				
	Bogue phase calculation (in weight %) *			
C_3S	53	-	-	
C_2S	17	-	-	
C_3A	7	-	-	
C ₄ AF	9	-	-	
	Physical and mechanical properties			
Fineness /	$401 \text{ m}^2/\text{kg}$	$d_{50} = 12.8 \mu m$	$d_{50} = 23.7 \mu m$	
Particle size		$d_{90} = 43.4 \mu m$	$d_{90} = 59.8 \mu m$	

*Cement chemistry notation used here, C=CaO, S=SiO₂, A = Al₂O₃, F = Fe₂O₃.

3.2 Sample preparation

Fifteen cementitious paste mixtures were prepared with varying fly ash content for two different fly ashes. The mixture proportions are shown in Table 2. The pastes were mixed using the following procedure [76]. Dry cement and fly ash were mixed for 90 seconds at 300 revolutions per minute (rpm) in a programmable vacuum mixer (Renfert Inc.) at a 70% vacuum level to ensure a good dispersion of fly ash within the binder powder. De-ionized water was

then added to the powder, and the vacuum mixer was operated at 400 ± 5 rpm for 90 seconds. The mixer was then stopped for 15 seconds, and any paste that may have collected on the sides and roof of the mixing bowl was scraped back into the bulk of the mixing bowl. The paste was then vacuum mixed for another 90 seconds at 400 ± 5 rpm.

The paste was cast into molds and sealed with their lids and duct tape to prevent the loss of moisture. Two sizes of molds were used depending on the experiments: 25.4mm × 50.8mm (1in × 2in) and 50.8mm × 101.6mm (2in × 4in), as described in Table 3. Immediately after sealing the molds, all cement paste samples were rotated for 24±2 hours on a roller at a speed of 50 rpm at 23±2°C to minimize bleeding. After rolling, the samples were cured in a sealed condition in an oven at 50±2°C for 18 days (equivalent to 56 days curing at 23°C, as calculated using the Arrhenius equation [77]).

Table 2. Mixture proportions (weight percentage) of the cement paste samples

Mixture	Water to	Cement	Fly Ash	Fly Ash
Number	binder ratio	(mass %)	(mass %)	name
	(w/b)			
1	0.35	100	0	-N/A-
2	0.35	80	20	Fly Ash 1
3	0.35	60	40	Fly Ash 1
4	0.45	100	0	-N/A-
5	0.45	80	20	Fly Ash 1
6	0.45	60	40	Fly Ash 1
7	0.55	100	0	-N/A-
8	0.55	80	20	Fly Ash 1
9	0.55	60	40	Fly Ash 1
10	0.35	80	20	Fly Ash 2
11	0.35	60	40	Fly Ash 2
12	0.45	80	20	Fly Ash 2
13	0.45	60	40	Fly Ash 2
14	0.55	80	20	Fly Ash 2
15	0.55	60	40	Fly Ash 2

252 3.3 Experimental program

The experimental program conducted in this study is summarized in Table 3. The details of each experiment will be described in the following sections.

 Table 3. Experimental program

Measured parameters	Experiment name	Number of samples tested	Size of the cylindrical molds
Non-evaporable water	Thermogravimetric analysis (TGA) [78]	5	25.4 mm in diameter 50.8 mm in height
CH content	Thermogravimetric analysis (TGA) following [78]	5	25.4 mm in diameter 50.8 mm in height
Porosity	Vacuum saturation following AASHTO TP 135-20 [79]	5	50.8 mm in diameter 101.6 mm in height
Bulk resistivity	Uniaxial measurements using AASHTO TP 119-20 Option A [80]	5	50.8 mm in diameter 101.6 mm in height
Compressive strength	ASTM C-39	5	50.8 mm in diameter 101.6 mm in height

3.4 Quantification of non-evaporable water and CH content

Thermogravimetric analysis (TGA) was performed to determine the amount of non-evaporable water as well as the CH content in the cementitious pastes. The sample for the TGA consisted of a powder sample of 20-30 mg taken from the hydrated cement paste that was ground and passed through a 75-micron sieve. The sieved powder was placed in a platinum crucible and loaded in the TGA instrument. The sample was first kept at 23°C for 3 minutes and then heated up to 990°C at 10°C/min under a nitrogen purge [78]. The mass loss was recorded at 0.5 second intervals during the experiment. The non-evaporable water content was quantified using equation (10):

$$w_n = \frac{m_{105^{\circ}C} - m_{1000^{\circ}C} \times (1 + (1 - r_{SCM}) \cdot LOI_{cem} + r_{SCM} \cdot LOI_{ash})}{m_{1000^{\circ}C} \times (1 + (1 - r_{SCM}) \cdot LOI_{cem} + r_{SCM} \cdot LOI_{ash})}$$
(10)

where $m_{105^{\circ}C}$ and $m_{1000^{\circ}C}$ are the sample masses recorded by the TGA at 105°C and 1000°C respectively, LOI_{cem} and LOI_{ash} represent the loss on ignition of the cement and fly ash used respectively (listed in Table 1), and ' r_{SCM} ' is the mass replacement of cement with fly ash in the cementitious system.

The mass of CH is computed using equation (11) [78].

$$m_{CH} = \frac{74.1}{18} \times \frac{m_{CH}^{start} - m_{CH}^{end}}{m_b^{init}} + \frac{74.1}{100} \times \left[\frac{100}{44} \times \frac{m_{CaCO3}^{start} - m_{CaCO3}^{end}}{m_b^{init}} - m_{CaCO_3}^{init} \right]$$
(11)

where m_{CH}^{start} and m_{CH}^{end} are the sample masses (g) recorded during the TGA at the start point $(365 \pm 7^{\circ}\text{C})$ and the endpoint $(445 \pm 7^{\circ}\text{C})$ of decomposition of Ca(OH)₂ respectively, m_{CaCO3}^{start} and m_{CaCO3}^{end} are the sample masses (g) recorded during the TGA at the start point $(576 \pm 13^{\circ}\text{C})$ and the endpoint $(661 \pm 12^{\circ}\text{C})$ of decomposition of CaCO₃ respectively, m_b^{init} is the initial anhydrous mass of the binder in the TGA, and $m_{CaCO_3}^{init}$ is the initial CaCO₃ content of the binder (in g/g_{binder}). The start and endpoint of decomposition of both CaCO₃ and Ca(OH)₂ were determined based on the second derivative curve of the sample's weight loss recorded during the TGA test with respect to temperature [78]. For the decomposition of each compound (Ca(OH)₂, CaCO₃), the second derivative curve displays one major positive peak and one major negative peak. The start point of the decomposition is the start point of the positive peak, and the endpoint of the decomposition is the endpoint of the negative peak. The ratio of 74.1/18 is the ratio of the molar mass of Ca(OH)₂ and the molar mass of water. The ratios of 74.1/100 and 100/44 are the molar weight ratios of Ca(OH)₂ to CaCO₃ and CaCO₃ to CO₂, respectively.

3.5 Porosity Tests

Porosity samples were demolded after the curing period and saturated with a simulated pore solution at 7 ± 2 torr (933 \pm 27 Pa) in a vacuum saturator according to the procedure described in AASHTO TP 135-20 [79]. The simulated pore solution consists of 7.6g/L NaOH

288 (0.19M), 10.64g/L KOH (0.19M) and 2g/L Ca(OH)₂ (0.027M). The hardened paste samples 289 were kept immersed in the solution for 48 ± 4 hours after being removed from the vacuum 290 saturator.

The porosity of the paste (ϕ_{paste}) is then calculated according to equation (12).

$$\phi_{paste} = \frac{w_{SAT} - w_{DRY}}{w_{SAT} - w_{APP}} \tag{12}$$

where w_{SAT} is the saturated surface-dry weight, w_{APP} is the weight of the sample measured underwater (also called apparent weight), and w_{DRY} is the oven-dry weight of the sample, obtained by keeping the samples in an oven at $105 \pm 2^{\circ}$ C until a constant mass was reached (i.e. the difference between any two successive values collected at least 24 hours apart is less than 0.1 % of the lowest value obtained).

3.6 Compressive Strength Tests

The compressive strength was determined in accordance with ASTM C39/C39M-18. Five cylinders were tested to determine the compressive strength of the mixtures. The cylinders were loaded at a rate of 241±14 kPa/s (35±2 psi/s) in a 3111 kN (700 kip) hydraulic compression machine, utilizing neoprene end caps when tested

3.7 Bulk Resistivity Tests

Uniaxial resistivity measurements were tested after the saturation at a single frequency of 1 kHz according to AASHTO TP 119-20 Option A [80]. The geometry of the sample, the temperature, and the phase angle were recorded during the resistance measurements [81]. The bulk resistivity (ρ_{bulk}) is calculated according to equation (13).

$$\rho_{bulk} = \left[\left(R_s \frac{A}{L} \right) \cos(\Phi) \right] e^{\left[\frac{E_{A-cond}}{R} \left(\frac{1}{T} - \frac{1}{T_0} \right) \right]}$$
(13)

where R_s is the measured bulk resistance of the sample (in Ω), A is the cross-sectional area of the sample (in m^2), and L is the length (m) of the sample, Φ is the measured phase angle (in

radians), E_{A-cond} is the activation energy of conduction (considered to be 15 kJ/mol [82]), R is the universal gas constant (8.314 J/mol-K), T is the sample temperature (in K), and T_0 is the reference temperature (298.15 K). Since the samples were vacuum saturated, the resistivity of the pore solution was known ($\rho_{ps} = 0.127\Omega m$), and the saturated formation factor (F_{SAT}) can be calculated according to equation (6) [65, 83].

4 RESULTS AND DISCUSSION

The results presented here are intended to demonstrate the predictions of performance parameters through the developed model and their comparison to experimental data. Furthermore, the effect of fly ash addition on pore refinement is discussed.

4.1 Non-Evaporable Water

As explained in section 2.2, the degree of reaction of the system (DOR_{sys}) was estimated based on the non-evaporable content as measured using mass change from the TGA. Figure 2 shows the non-evaporable water for the two fly ashes used in this study as well as the determined DOR_{sys}. As the w/b increases, the non-evaporable water content increases due to an increase in both, the hydration of OPC and the reaction of fly ash in the system. This is also seen as an increase in the DOR_{sys}. It should be noted that while Fly Ash 1 seems to deviate from this trend (i.e., there is a slight decrease in the non-evaporable water) at a replacement of 20% for w/b 0.45 and w/b 0.55, the measured values of non-evaporable water (and sthe calculated values of DOR_{sys}) lie within the standard error of measurement. The observed difference between the means of the two measured values of non-evaporable water are 0.7g/100g_{binder} (and the corresponding difference in the DOR_{sys} is 3%), lower than the standard experimental error (which is 1.0g/100g_{binder} corresponding to a DOR_{sys} of 3%). For the fly ash of higher reactivity (Fly Ash 1), as the replacement level is increased, the non-evaporable water remains nearly constant due to increased hydration due to the filler effect compensating the

dilution. This is also seen as the DOR_{sys} increasing due to an increase in the degree of hydration of cement and the degree of reaction of the fly ash. As the replacement of cement with ash increases, the non-evaporable water content for the fly ash of lower reactivity (Fly Ash 2) decreases due to dilution of OPC with a lower reactive material. This is also seen as the decrease in the DOR_{sys} .

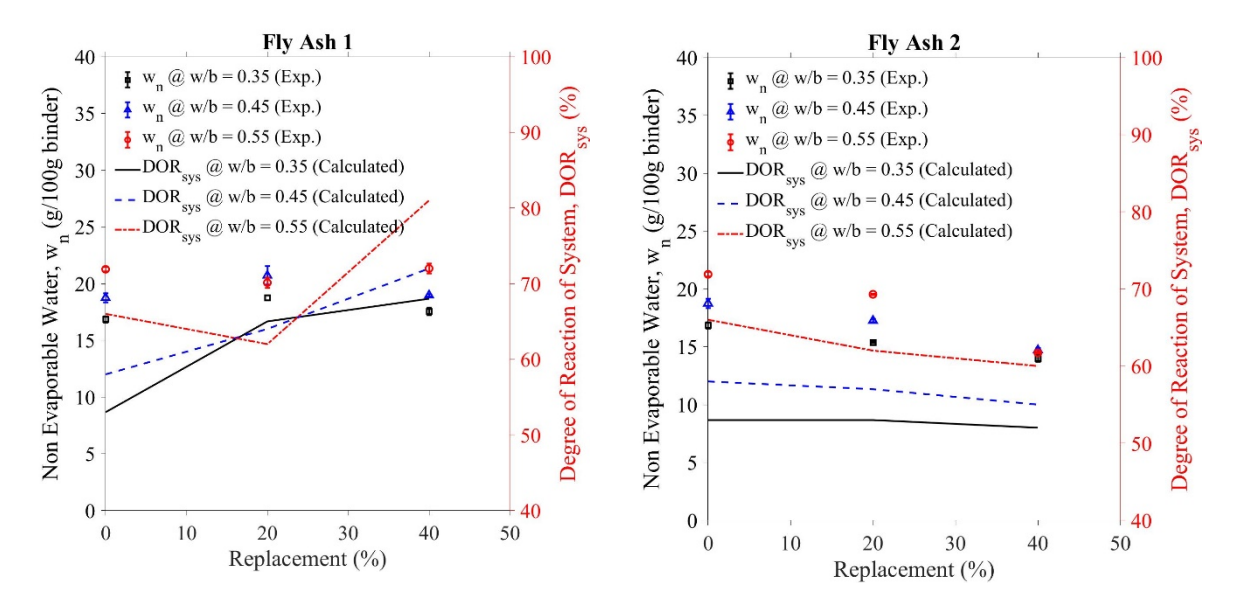


Figure 2. Non-evaporable water content in the cementitious systems studied.

4.2 Calcium Hydroxide

Figure 3 shows the predicted CH content in the systems studied, and the experimentally determined mass of CH. For both fly ashes, as the w/b of the system increases, the mass of CH in the system increases (with the exception of Fly Ash 1 w/b 0.55 40% fly ash). This can be attributed to the increased degree of reaction of the system at a given time in systems with higher w/b. As the replacement of cement with fly ash increases, the mass of CH in the paste decreases. This is a result of the pozzolanic reactions of the ash, which consume CH. This is supported by the data, which shows the more reactive fly ash (Fly Ash 1) consuming more CH than the lower reactivity fly ash (Fly Ash 2).

The model predicts the masses of CH with an error of $3.1g/100g_{binder}$ ($\approx 16\%$) for OPC systems and $5.2g/100g_{binder}$ ($\approx 39\%$) for the OPC + 20% Fly Ash systems, and $6.1g/100g_{binder}$ ($\approx 91\%$) for the OPC + 40% Fly ash systems studied. It is worth noting that the model underpredicts the mass of CH in the system, with an increase in the error between the model and the experiments at higher replacement levels. This is likely a result of the combination of (i) the calculation of the DOR_{sys} from experimentally determined non-evaporable water (the GEMS/CEMDATA v18 framework predicts a higher amount of w_n than what is measured in experiments [37, 84]). (ii) Some studies have also shown that the CH is never truly depleted in even mature OPC+SCM systems which have been hydrated for over a year ([85-88]), which could corroborate the hypothesis that the CH might not be fully available to react, which might contribute to the overprediction of the CH consumption because the thermodynamic calculations assume that all CH is available to react [46].

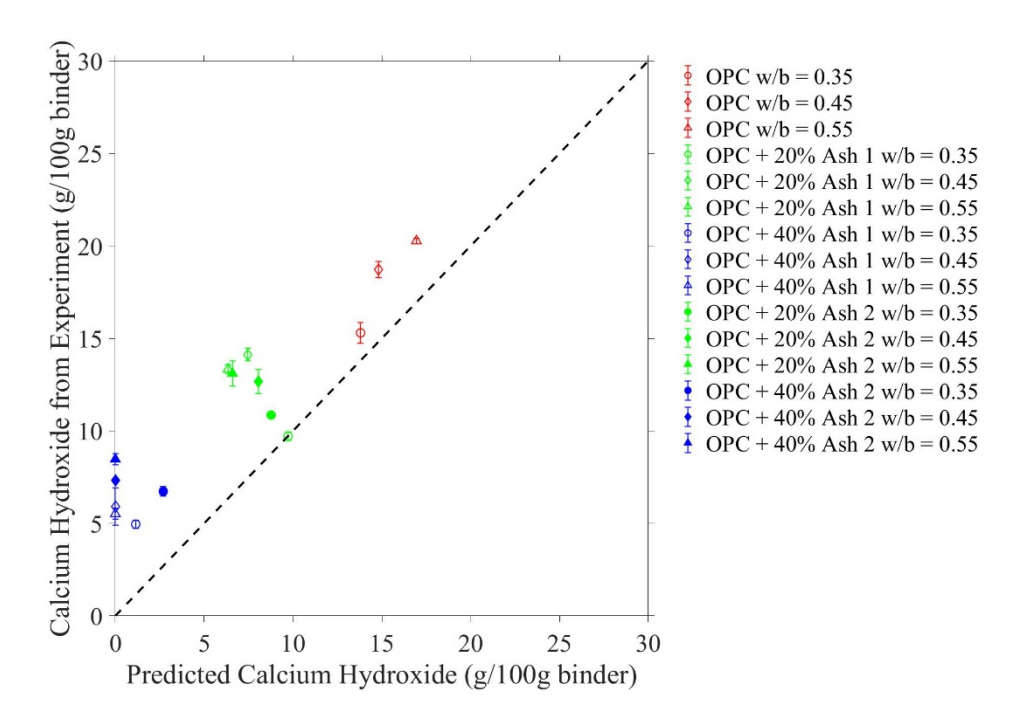


Figure 3. A Comparison between the predicted mass of CH in the system and the mass of CH measured using TGA for the two fly ashes chosen for the study.

4.3 Porosity

The total porosity of hydrated cement pastes (ϕ_{paste}) may be calculated using equation (2) as the sum of volumes of gel water, capillary water, pores due to chemical shrinkage and air voids. In this work the pastes were vibrated until all the air voids were removed, and as such, the volume of entrapped air is set to 0%. Figure 4 shows the results of the model as compared with the experimentally measured values.

An increase in the w/b causes an increase in the total porosity of the system. This is due to the higher volume of capillary pores in the system. An increase in the replacement of cement with fly ash also causes the porosity of the system to increase, which is consistent with the literature [32, 89-92]. This is due to an increase in the volume of capillary pores in the system due to dilution effects, which is caused by the substitution of highly reactive OPC with a less reactive binder component (fly ash). This is further supported by the Figure 4, where Fly Ash 2 (the fly ash of lower reactivity) shows a higher increase in porosity with an increase in replacement than Fly Ash 1 (higher reactivity fly ash).

The model predicts the porosity with a percentage error of 5%. The percentage error for OPC systems is 5%, for OPC + 20% FA systems is 6% and for OPC + 40% FA systems is 5%. In most cases, the porosity predicted by the model is lower than that predicted by experiments, consistent with the literature [30]. This is likely due to the GEMS/CEMDATA framework used. In the model, for a given C/S ratio of C-S-H, the H/S of the C-S-H is higher than what is seen in the experiments [37, 84]. A higher H/S in the model means that the model predicts more bound water in the C-S-H, which results in a lower predicted volume of gel water, and consequently, the model predicts a lower porosity.

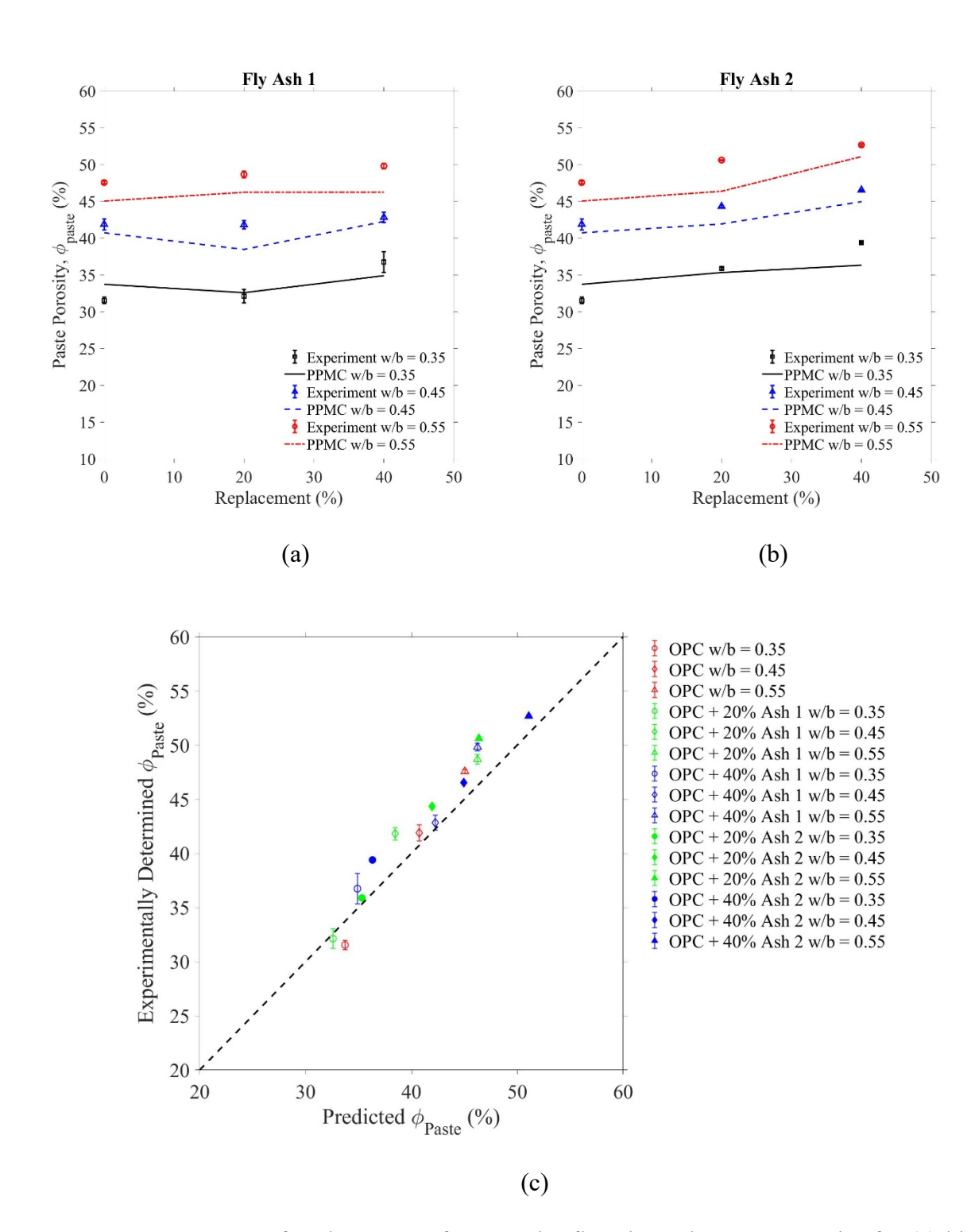


Figure 4. Impact of replacement of cement by fly ash on the paste porosity for (a) high reactivity ash ($DOR^* = 52\%$) and (b) low reactivity ash ($DOR^* = 23\%$).

4.4 Compressive Strength

389

390

391

392

393

394

395

396

397

398

399

400

401

402

403

404

405

406

407

408

409

410

411

412

413

As discussed in Section 2.4.3, Powers and Brownyard's gel-to-space ratio is used to calculate the compressive strength of cementitious systems. Figure 5 plots a comparison between the predicted strength and the experimentally obtained values of compressive strength. An increase in the w/b from 0.45 to 0.55 decreases the compressive strength of the system consistent with the trends predicted by the model. This is due to the more significant fraction of capillary pores (which are larger in size than gel pores). However, the sample with the lowest w/b (0.35) deviated from the model predictions due to possible insufficient consolidation (lack of using a water reducer or a dispersion agent); the model predicts an increase in the compressive strength while the experiments show that the compressive strength remains nearly constant as the w/b is decreased from 0.45 to 0.35. The system may contain entrapped air which is not included in thermodynamic calculations. This could be a reason for why the model constantly underpredicts the porosity by 1-3% (Figure 4(c)). As the replacement of OPC with Fly Ash 2 (DOR*=23%) increases, the compressive strength decreases. This can be explained by the replacement of highly reactive OPC with a binder of lesser reactivity. One seeming exception to this is the paste made of Fly Ash 2, w/b 0.35, where the strength increases and then decreases, which is hypothesized to be due to the low w/b preventing the formation of a significant volume of large capillary pores. For the higher reactivity fly ash (Fly Ash 1, DOR*=52%), except for the w/b 0.35 mixtures (where consolidation issues are suspected), an increase in replacement of OPC with the fly ash causes an increase in the compressive strength. This is hypothesized to be due to the pozzolanic reactions causing a decrease in the size of capillary pores in the system (as evidenced by literature on OPC+SCM systems [34, 35]). In other words, while the total volume of capillary pores increases, the volume fraction of larger capillary pores decreases, and the volume fraction of smaller pores increases (also known as "pore refinement").

The model captures the behavior of the pastes with an error of 11.7 MPa (\approx 23%). The error for OPC systems is 6.2MPa (\approx 14%), for OPC + 20% FA systems is 12.2MPa (\approx 25%), and for OPC + 40% FA systems is 15.0MPa (\approx 28%). It can also be seen that in most cases, the model underpredicts the compressive strength, and the error increases as the replacement of OPC with fly ash increases. This is likely because the value of the constant ($a_1 = 138$ MPa) used in equation (4) for calculating the strength from the gel-to-space ratio is kept the same for OPC and OPC+FA systems. Powers and Brownyard [12] hypothesized that the value of a_1 depends on the intrinsic strength of the gel. The value of a_1 could vary as different hydration products form in OPC+FA systems as different pore size distributions occur [34, 35]. As such, more work is needed in predicting the strength of OPC+FA systems where the pore size distributions are likely to deviate from plain OPC systems, and micromechanical approaches show promising results [55, 93, 94].

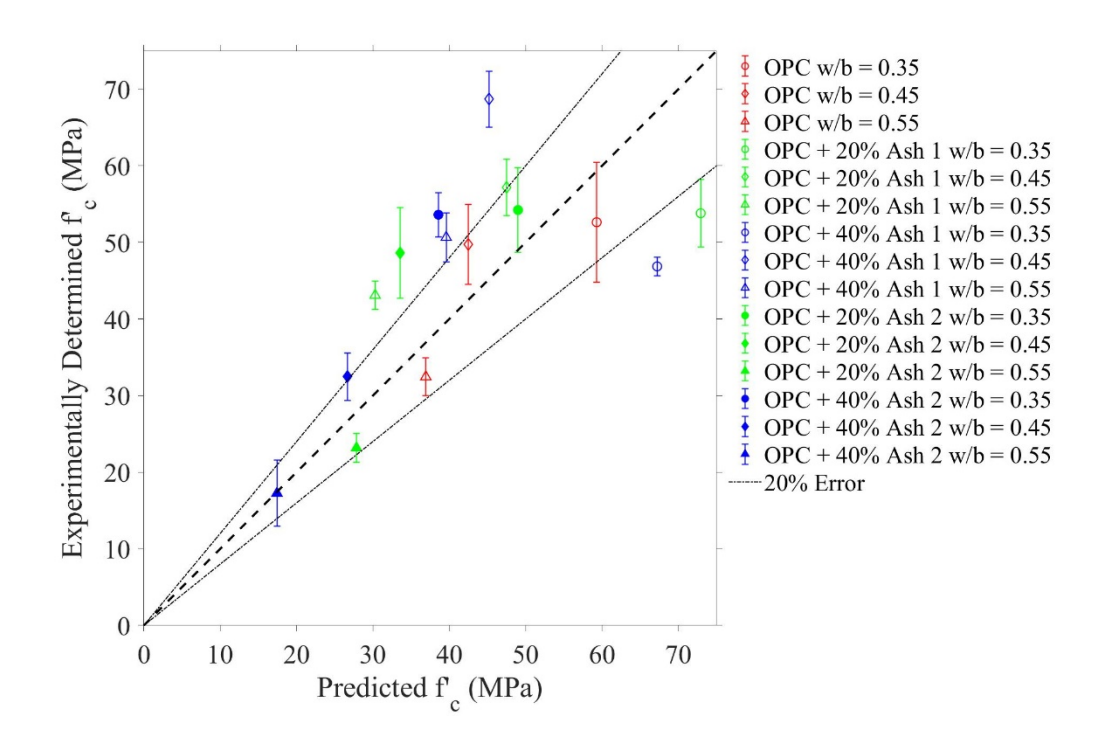
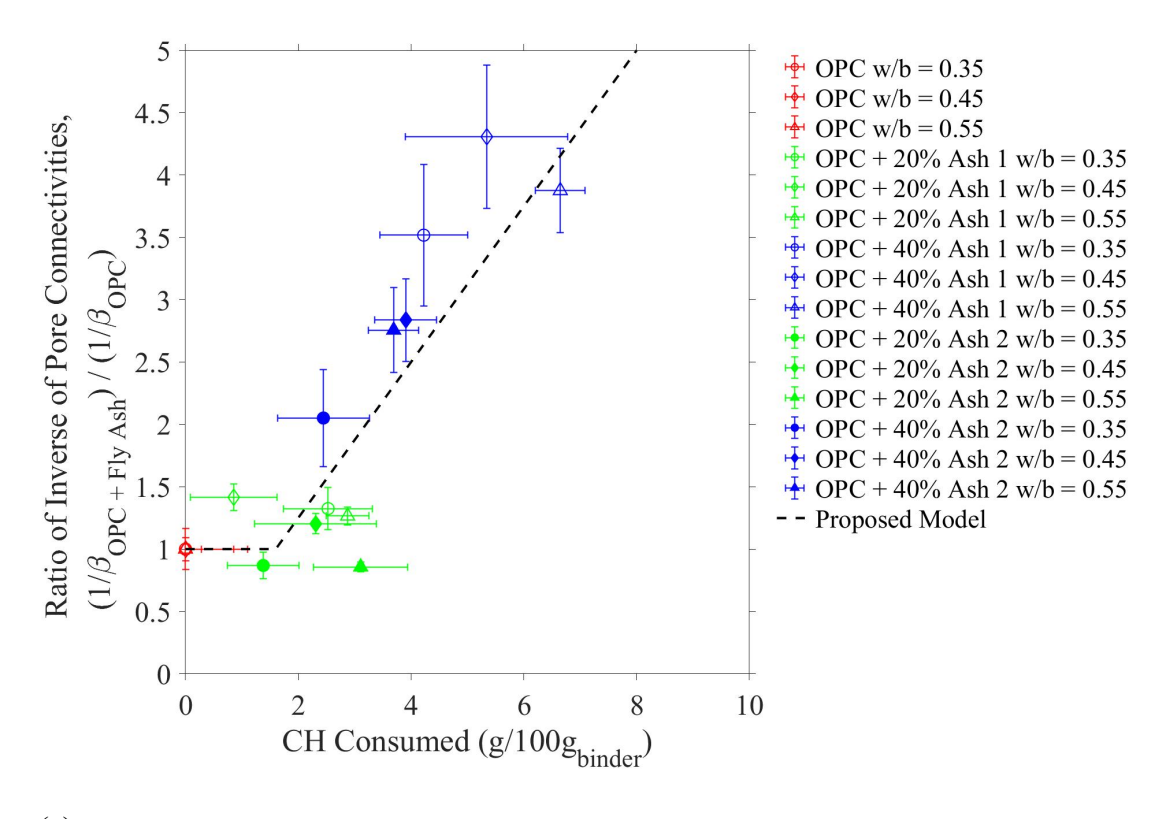


Figure 5. A Comparison between the predicted compressive strength (using the gel-space ratio) and the experimentally determined strength of the pastes for the two fly ashes chosen for the study.

4.5 Pore Connectivity and a Proposed Model to Quantify its Refinement

The pore connectivity of the cementitious system is a measure of transport properties of porous materials. It is used to calculate the formation factor using equation (5). The PPMC model predicts the formation factor by calculating the porosity (using equation (2)), and then uses the determined pore volumes to predict pore connectivity (using equations (7) to (9)). One assumption of the existing PPMC model is that the constants (b_1 and b_2 in equation (9)), which are used to predict the pore connectivity of cementitious pastes, have the same values for both OPC and OPC+FA systems. Practically speaking, this assumption means that the pore size distributions are assumed to remain the same for both pastes made of OPC and pastes made of OPC+SCMs. It has been shown in the literature that in systems with SCMs such as fly ash, the pore structure becomes more refined [33, 35, 36, 95, 96]: the volumes of coarser capillary pores reduce, and finer capillary pores increase. In this work, we provide an empirical equation to quantify the extent of pore refinement as a function of CH consumption (which can be related to DOR* and the replacement level of OPC with SCM).

Figure 6 (a) is a plot of the ratio of the inverse of the experimentally measured pore connectivity of OPC+FA systems to the inverse of the experimentally measured pore connectivity of OPC systems as a function of CH consumption. An increase in the consumption of CH causes an increase in the ratio of the pore connectivity of OPC to the pore connectivity of OPC+FA systems. This means that as more CH is consumed (such as when a more reactive fly ash is used), the pore structure becomes more refined, and the pore connectivity of the OPC+FA system decreases. The x-axis of Figure 6 (a) is the CH consumed and is, therefore, a measure of the extent of the pozzolanic reaction that occurs. An increase in the amount of ash causes more consumption of CH due to the presence of a higher volume of reactive silica. Higher reactivity fly ash consumes more CH at the same replacement level than lower reactivity fly ash, due to the increase in the amount of silica available to react with the CH.





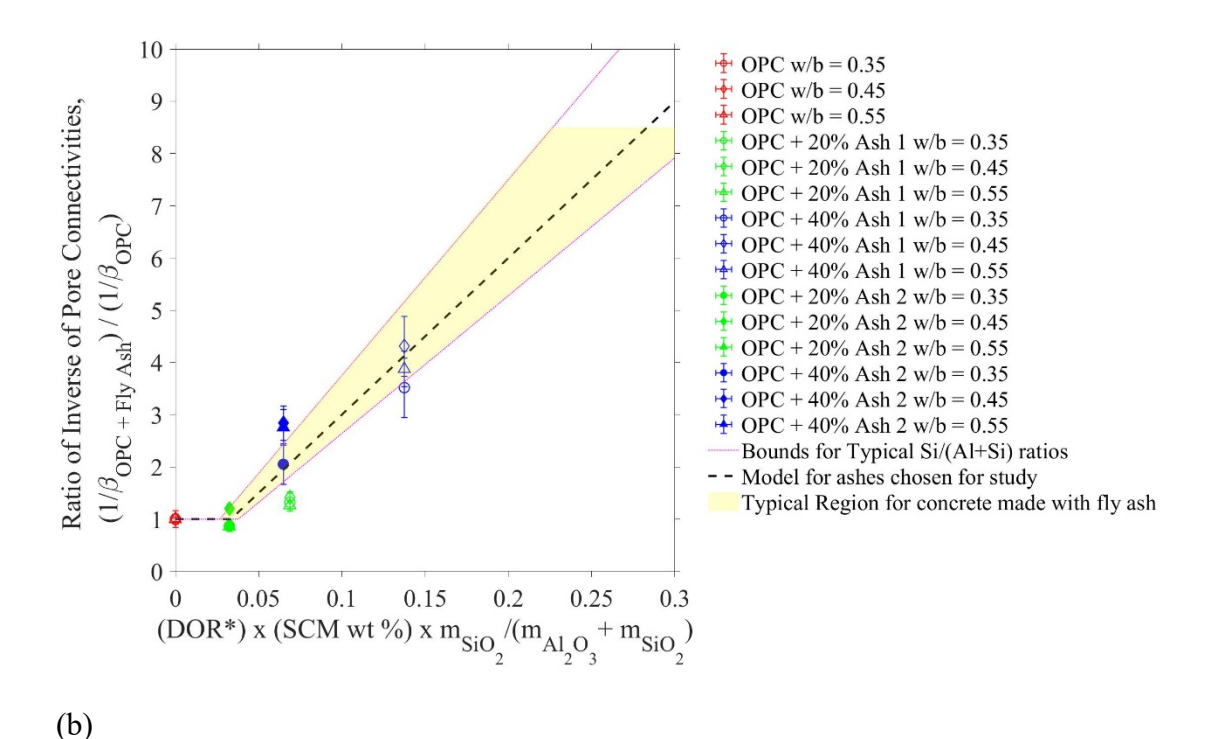


Figure 6. (a) A measure of pore refinement as a function of the CH consumed (b) An approximate way to estimate the pore refinement using the fly ash reactivity, weight replacement, and fly ash chemistry.

Figure 6 (a) also shows a proposed empirical modification to determine the pore connectivity using the PPMC model (the dashed line in the plot) to capture the extent of pore refinement, 459 shown mathematically in equation (14). The line was obtained by visual fitting to the experimental data points.

457

458

460

461

462

463

464

465

466

467

468

469

470

471

472

473

474

475

476

477

478

479

$$\chi_{pore\ ref} = \frac{1/\beta_{OPC+SCM}}{1/\beta_{OPC}} = 0.625 m_{CH\ consumed} \ge 1$$
 (14)

where $\chi_{pore\ ref}$ denotes the extent of pore refinement in the system, $\beta_{OPC+SCM}$ is the pore connectivity of the OPC+SCM system, β_{OPC} is the pore connectivity of the OPC system made of the same w/b at the same age, and $m_{CH\ consumed}$ is the mass of CH consumed (due to pozzolanic reactions).

From Figure 6 (a), it can be seen that pore refinement occurs beyond 2-4 g of CH consumption per 100 g binder. This could be because a certain amount of minimum pozzolanic reaction is necessary for pore-discontinuity to occur. In the model, owing to the overprediction of CH consumption by up to 4g/100g_{binder}, pore refinement was considered to occur if the mass of CH consumed in the system was greater 4.5g/100gbinder.

In this work the mass of CH consumed in the OPC+FA pastes was measured by determining mass change using the TGA. An alternate method to estimate the pore refinement is also shown in Figure 6 (b). The figure shows a plot of a measure of pore refinement plotted against the product of the reactivity of the ash, the mass replacement of OPC with fly ash, and the mass ratio of SiO₂ to SiO₂+Al₂O₃ in the ash, which yields a quantity that is related to CH consumption. Since all the components forming this quantity are either easily measurable or can be obtained from mill certifications, the plot provides a practical tool to relate pore connectivity to CH consumption without the need to measure CH consumption. An approximate model to calculate the extent of pore refinement using these parameters is also plotted (black dashed line), shown in equation (15) below.

$$\chi_{pore \ ref} = \frac{1/\beta_{OPC + SCM}}{1/\beta_{OPC}} = 30 \cdot DOR^* \cdot r_{SCM} \cdot \frac{m_{SiO_2}}{m_{SiO_2} + m_{Al_2O_3}} \ge 1$$
 (15)

where $\beta_{OPC+SCM}$ is the pore connectivity of the OPC+SCM system, β_{OPC} is the pore connectivity of the plain OPC system made of the same w/b at the same age, DOR^* is the measured reactivity of the fly ash, r_{SCM} is the mass replacement of OPC with fly ash, and m_{SIO_2} and $m_{Al_2O_3}$ are the mass fractions of SiO₂ and Al₂O₃ respectively in the fly ash (which can be obtained from the mill certificate of the ash). Figure 6 (b) also shows the predicted typical upper and lower bounds for the pore refinement when the mass ratio of SiO₂ to SiO₂+Al₂O₃ varies in a fly ash for any given DOR* and replacement level, represented by the pink dotted line. The mass ratio of SiO₂ to SiO₂+Al₂O₃ typically lies between 60% and 75% [16, 17, 75, 97-100]. As seen, most data points lie within a margin of error within the predicted bounds. Figure 6 (b) also shows the range of expected values of pore refinement for concrete made of fly ashes (typically DOR* of fly ashes are between 20% and 75% [16, 17, 75, 97-100], and typical mass replacement levels are considered to be between 20%-40% [101].

4.6 Formation Factor

The formation factor is calculated from the original PPMC model proposed in [32] and after applying the empirical pore refinement model (equation (14)). Figure 7 (a) and (b) plot the impact of replacement of cement by fly ash on the formation factor of hydrated paste for the two fly ashes chosen for the study, with the thinner dotted lines representing the PPMC model (without pore refinement), and the thicker lines representing the model with the pore refinement. As shown in Figure 7 (a) and (b), as the w/b increases, the formation factor decreases. This is attributed to the increase in porosity and pore connectivity in systems with higher w/b. For both ashes, as the replacement of cement with fly ash increases, the formation factor first stays nearly constant, then increases, and then decreases. This can be explained by a combination of the effects of dilution, lack of reaction of fly ash, and pore refinement. At low

replacement levels, the amount of CH consumed is not enough to cause any significant pore refinement in the system. As the replacement of cement with fly ash is increased, capillary porosity of the system increases (as seen in Figure 4 (a) and (b)), but there is also a significant amount of pore refinement occurring because of the redistribution of porosity caused by pozzolanic reactions. Beyond a certain replacement level however, the dilution of cement with fly ash causes a significant increase in the capillary porosity, and the complete consumption of CH prevents any further pore refinement from occurring. Therefore, the formation factor at high replacements of cement with fly ash are quite low.

Another important use of the developed model is the potential to determine the optimal replacement of cement with fly ash in an OPC+FA system. The formation factor may be maximized at a certain replacement level for a given w/b, for example, in the case of Fly Ash 1, the optimal replacement level of cement with fly ash at a w/b of 0.45 appears to be 30%. It must be noted that the simulations were run at every 10% intervals, and running the model over smaller intervals may yield more accurate values.

The original PPMC model which was proposed [32] was used to predict the formation factor of the mixtures. The original model appears to work reasonably well for the OPC systems, with an error in prediction of 12% for the OPC systems, and 19% for the OPC + 20% FA systems. At higher replacement levels (OPC + 40% FA) the error in predicting the formation factor is higher at 72%. The proposed modification to the PPMC, to quantify pore refinement, significantly reduces the error (from 72% to 52%). It should be noted that the apparently high error is observed for the formation factor in OPC+20% FA mixtures with a w/b of 0.55 may be due to the overprediction of CH consumption. Note that this work also only considers the chemical effects and the reactivity of the fly ashes in the study, and further work is needed to assess the influence of other parameters such as the packing effects and heterogeneity of mixing on the pore connectivity and formation factor of cementitious systems.

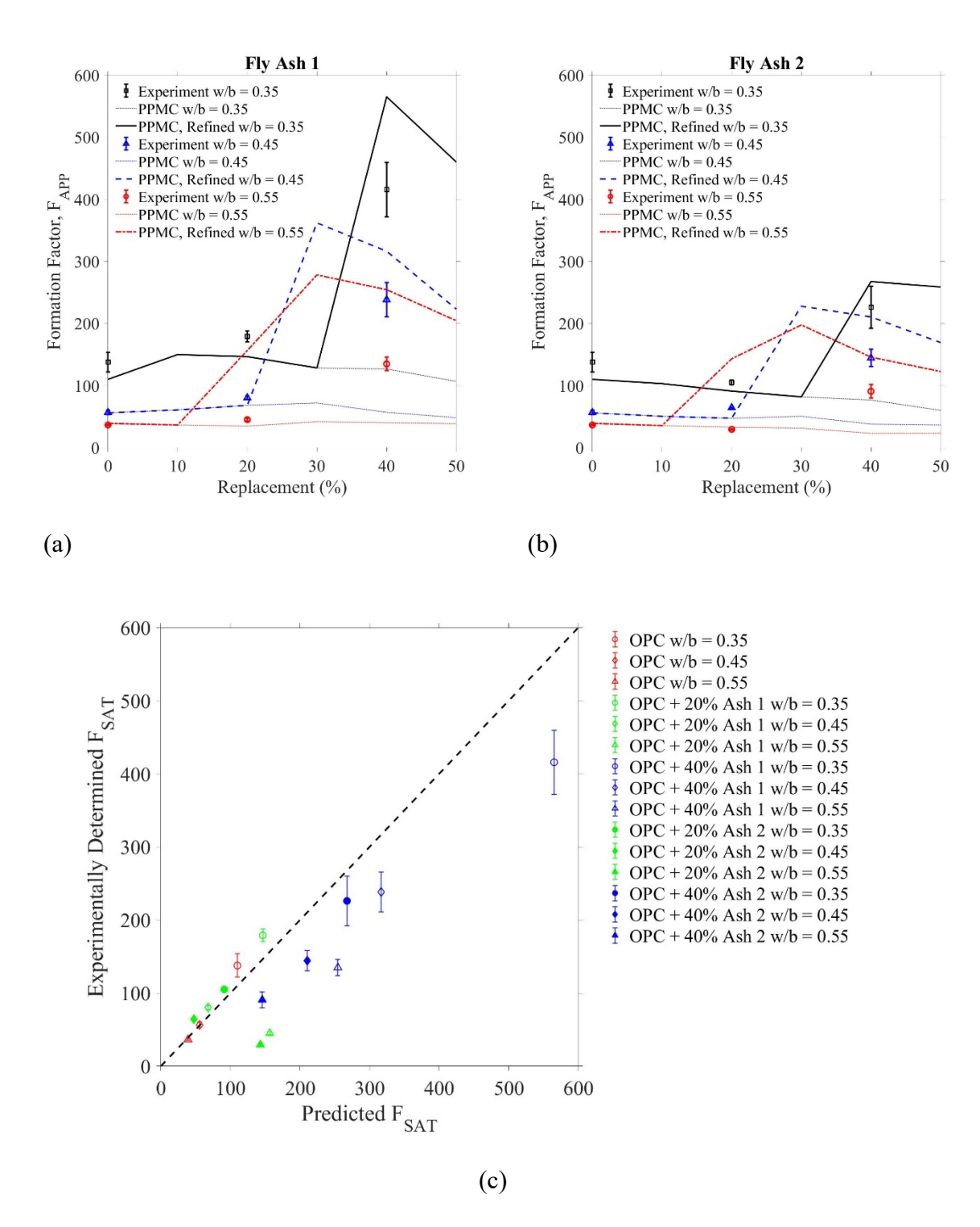


Figure 7. Impact of replacement of cement by fly ash on Formation Factor for (a) high reactivity ash (DOR = 52%) and (b) low reactivity ash (DOR = 23%). (c) Comparison of the experimentally determined and predicted formation factor for all mixtures.

5 CONCLUSIONS

This paper describes an approach to use thermodynamic modeling and a pore partitioning model to predict the CH content, porosity, strength, and formation factor of hydrated pastes made of OPC and OPC + Fly Ash. Two ashes were chosen for the study with two different reactivities. The CH content is predicted to within 4g/100g_{binder} for all ashes, and any errors appear to be mostly due to the physical availability of the CH in the experiments. An increase in the replacement of OPC with fly ash decreases the CH content in the pastes. A higher reactivity fly ash depletes more CH in the OPC + fly ash pastes than a lower reactivity fly ash.

A pore partitioning model is also used with thermodynamic models to predict the porosity and pore volumes of OPC and OPC + fly ash systems. The predictions of porosity are within 5% error for the two fly ashes chosen for the study and are consistent with the trends observed in the literature. An increase in w/b increases the total porosity of the paste, as does an increase in the fly ash replacement level.

A framework to couple thermodynamic modeling with Powers and Brownyard's gel-space ratio to determine the compressive strengths of cementitious systems is also outlined. The compressive strength is predicted with an RMS error of 11.5 MPa (the error for OPC systems is 6.2MPa (\approx 14%), for OPC + 20% FA systems is 12.2MPa (\approx 25%), and for OPC + 40% FA systems is 15.0 MPa (\approx 28%)). An increase in w/b decreases the compressive strength of hydrated paste. For a higher reactivity ash, an increase in replacement increases strength. For an ash of low reactivity, the compressive strength decreases due to an increase in the total capillary porosity of the system. As such, work is needed in this area to predict strengths more accurately, and micromechanical models show promising results.

This paper describes a method to predict the formation factor of hydrated pastes made of OPC and OPC + fly ash. An empirical model to quantify pore refinement when a SCM such as fly ash is used is also proposed based on experimental data. The error in the predictions of formation factor using the proposed approach (PPMC + pore refinement) for the w/b of 0.35 and 0.45 is between 1-20% for OPC systems, 13-26% for the OPC+20% FA systems, and 18-46% for the OPC+40% FA systems. The errors for the w/b = 0.55 system are higher, especially with higher volumes of ash that requires additional research. It seems that the higher errors are associated with an overprediction in the mass of CH consumed. An increase in the w/b decreases the formation factor. As the replacement of cement with fly ash increases, the formation factor first remains nearly constant, then increases and then decreases. This is possible due to the competing effects of dilution (mainly an increasing capillary porosity) and pore refinement as more fly ash is added to the system. At low replacement levels, there is not enough pozzolanic reaction to cause pore refinement. As the amount of fly ash increases, the pozzolanic reactions increase, and this causes a significant amount of pore refinement to occur. At high replacement levels, the formation factor decreases due to an increase in capillary porosity. A framework is also outlined to optimize the use of fly ashes in cementitious mixtures to maximize the formation factor.

6 DECLARATION OF COMPETING INTEREST

The authors declare that they have no known competing financial interests or personal relationships that could have appeared to influence the work reported in this paper.

7 ACKNOWLEDGMENTS

553

554

555

556

557

558

559

560

561

562

563

564

565

566

567

568

569

570

573

574

575

576

The authors gratefully acknowledge the financial support provided by ARPA-E, Energy Power Research Institute (EPRI), and National Science Foundation (Grant number NSF CMMI 1728358). The authors gratefully acknowledge support from the John and Jean Loosely Chair

- and the Edwards Distinguished Chair at Oregon State, which have supported the last two
- authors, respectively. The authors also acknowledge fruitful discussions with Prof. Barbara
- 579 Lothenbach of EMPA, Switzerland, and discussions with Dr. Deborah Glosser of Oregon State
- 580 University. The authors also heartfully acknowledge Antara Choudhary of Oregon State
- University for her help with reactivity tests, and Siva Teja Chopperla of Oregon State
- University for his help with compressive strength testing. The authors also acknowledge the
- laboratory assistance of Keegan Zetterberg and Josephine Crofoot of Oregon State University.

584 8 REFERENCES

- [1] R. Feret, On the compactness of the mortars, Annales des Ponts et Chaussées, Série, 1892,
- 586 pp. 5-164.
- 587 [2] D.A. Abrams, Design of concrete mixtures, bulletin 1, Structural materials research
- laboratory. Chicago: Lewis Institute (1918).
- [3] J. Bolomey, Granulation et prévision de la résistance probable des bétons, Travaux 19(30)
- 590 (1935) 228-232.
- [4] A.M. Neville, Properties of concrete, Longman London1995.
- 592 [5] W.A. Gutteridge, J.A. Dalziel, Filler cement: the effect of the secondary component on the
- 593 hydration of Portland cement: part I. A fine non-hydraulic filler, Cement Concrete Res 20(5)
- 594 (1990) 778-782.
- 595 [6] K.L. Scrivener, B. Lothenbach, N. De Belie, E. Gruyaert, J. Skibsted, R. Snellings, A.
- Vollpracht, TC 238-SCM: hydration and microstructure of concrete with SCMs, Materials and
- 597 Structures 48(4) (2015) 835-862.
- 598 [7] V.G. Papadakis, Experimental investigation and theoretical modeling of silica fume activity
- in concrete, Cement Concrete Res 29(1) (1999) 79-86.
- [8] V.G. Papadakis, Effect of fly ash on Portland cement systems: Part I. Low-calcium fly ash,
- 601 Cement Concrete Res 29(11) (1999) 1727-1736.

- [9] V.G. Papadakis, Effect of fly ash on Portland cement systems: Part II. High-calcium fly
- ash, Cement Concrete Res 30(10) (2000) 1647-1654.
- 604 [10] V.G. Papadakis, S. Tsimas, Supplementary cementing materials in concrete: Part I:
- efficiency and design, Cement Concrete Res 32(10) (2002) 1525-1532.
- [11] B.S. EN, 206-1 Concrete-Part 1: Specification, performance, production and conformity,
- 607 British Standards Institution (2000).
- [12] T.C. Powers, Structure and physical properties of hardened Portland cement paste, Journal
- of the American Ceramic Society 41(1) (1958) 1-6.
- 610 [13] T.C. Powers, T.L. Brownyard, Studies of the physical properties of hardened Portland
- cement paste, Journal Proceedings, 1946, pp. 101-132.
- [14] P. Lura, O.M. Jensen, K. Van Breugel, Autogenous shrinkage in high-performance cement
- paste: An evaluation of basic mechanisms, Cement Concrete Res 33(2) (2003) 223-232.
- 614 [15] L. Lam, Y. Wong, C. Poon, Degree of hydration and gel/space ratio of high-volume fly
- ash/cement systems, Cement Concrete Res 30(5) (2000) 747-756.
- 616 [16] D. Glosser, A. Choudhary, O.B. Isgor, J. Weiss, Investigation of the Reactivity of Fly Ash
- and its Effect on Mixture Properties, ACI Materials Journal In Press (2019).
- 618 [17] P. Suraneni, J. Weiss, Examining the pozzolanicity of supplementary cementitious
- materials using isothermal calorimetry and thermogravimetric analysis, Cement and Concrete
- 620 Composites 83 (2017) 273-278.
- [18] D.P. Bentz, CEMHYD3D: A Three-Dimensional Cement Hydration and Microstructure
- 622 Development Modelling Package. Version 2.0 NIST, 2000.
- 623 [19] E.J. Garboczi, D.P. Bentz, The effect of statistical fluctuation, finite size error, and digital
- resolution on the phase percolation and transport properties of the NIST cement hydration
- 625 model, Cement Concrete Res 31(10) (2001) 1501-1514.

- 626 [20] K. Van Breugel, Numerical simulation of hydration and microstructural development in
- hardening cement-based materials (I) theory, Cement Concrete Res 25(2) (1995) 319-331.
- 628 [21] K. Van Breugel, Numerical-Simulation of Hydration and Microstructural Development in
- Hardening Cement-Based Materials .2. Applications, Cement Concrete Res 25(3) (1995) 522-
- 630 530.
- 631 [22] R. Chaube, T. Kishi, K. Maekawa, Modelling of concrete performance: Hydration,
- microstructure and mass transport, CRC Press1999.
- [23] T. Ishida, K. Maekawa, An integrated computational system of mass/energy generation,
- 634 transport and mechanics of materials and structures, Doboku Gakkai Ronbunshu 1999(627)
- 635 (1999) 13-25.
- 636 [24] K. Maekawa, T. Ishida, T. Kishi, Multi-scale modeling of concrete performance, Journal
- of Advanced Concrete Technology 1(2) (2003) 91-126.
- [25] S. Bishnoi, K.L. Scrivener, mu ic: A new platform for modelling the hydration of cements,
- 639 Cement Concrete Res 39(4) (2009) 266-274.
- [26] S. Bishnoi, K.L. Scrivener, Studying nucleation and growth kinetics of alite hydration
- using mu ic, Cement Concrete Res 39(10) (2009) 849-860.
- 642 [27] B. Lothenbach, D.A. Kulik, T. Matschei, M. Balonis, L. Baquerizo, B. Dilnesa, G.D.
- Miron, R.J. Myers, Cemdata 18: A chemical thermodynamic database for hydrated Portland
- cements and alkali-activated materials, Cement Concrete Res 115 (2019) 472-506.
- 645 [28] B. Lothenbach, T. Matschei, G. Möschner, F.P. Glasser, Thermodynamic modelling of
- the effect of temperature on the hydration and porosity of Portland cement, Cement Concrete
- 647 Res 38(1) (2008) 1-18.
- 648 [29] B. Lothenbach, F. Winnefeld, Thermodynamic modelling of the hydration of Portland
- 649 cement, Cement Concrete Res 36(2) (2006) 209-226.

- 650 [30] V.J. Azad, P. Suraneni, O. Isgor, W. Weiss, Interpreting the pore structure of hydrating
- cement phases through a synergistic use of the Powers-Brownyard model, hydration kinetics,
- and thermodynamic calculations, Advances in Civil Engineering Materials 6(1) (2017) 1-16.
- 653 [31] D. Glosser, V.J. Azad, P. Suraneni, B. Isgor, J. Weiss, An extension of the Powers-
- Brownyard model to pastes containing SCM, ACI Materials Journal in Press (2019).
- 655 [32] K. Bharadwaj, D. Glosser, M.K. Moradllo, O.B. Isgor, J. Weiss, Toward the Prediction of
- Pore Volumes and Freeze-Thaw Performance of Concrete Using Thermodynamic Modelling,
- 657 Cement Concrete Res 124 (2019) 105820.
- 658 [33] N. Neithalath, J. Persun, R.K. Manchiryal, Electrical conductivity based microstructure
- and strength prediction of plain and modified concretes, International Journal of Advances in
- Engineering Sciences and Applied Mathematics 2(3) (2010) 83-94.
- [34] P.K. Mehta, Studies on Blended Portland Cements Containing Santorin Earth, Cement
- 662 Concrete Res 11(4) (1981) 507-518.
- [35] P.K. Mehta, P.J. Monteiro, Concrete Microstructure, Properties and Materials, 2006.
- 664 [36] B. Lothenbach, K. Scrivener, R.D. Hooton, Supplementary cementitious materials,
- 665 Cement Concrete Res 41(12) (2011) 1244-1256.
- 666 [37] D.A. Kulik, Improving the structural consistency of CSH solid solution thermodynamic
- 667 models, Cement Concrete Res 41(5) (2011) 477-495.
- [38] D.A. Kulik, T. Wagner, S.V. Dmytrieva, G. Kosakowski, F.F. Hingerl, K.V. Chudnenko,
- 669 U.R. Berner, GEM-Selektor geochemical modeling package: revised algorithm and GEMS3K
- numerical kernel for coupled simulation codes, Computational Geosciences 17(1) (2013) 1-24.
- [39] B.Z. Dilnesa, B. Lothenbach, G. Le Saout, G. Renaudin, A. Mesbah, Y. Filinchuk, A.
- Wichser, E. Wieland, Iron in carbonate containing AFm phases, Cement Concrete Res 41(3)
- 673 (2011) 311-323.

- 674 [40] B.Z. Dilnesa, B. Lothenbach, G. Renaudin, A. Wichser, D. Kulik, Synthesis and
- characterization of hydrogarnet Ca3 (AlxFe1- x) 2 (SiO4) y (OH) 4 (3- y), Cement Concrete
- 676 Res 59 (2014) 96-111.
- 677 [41] B.Z. Dilnesa, B. Lothenbach, G. Renaudin, A. Wichser, E. Wieland, Stability of
- 678 monosulfate in the presence of iron, Journal of the American Ceramic Society 95(10) (2012)
- 679 3305-3316.
- [42] F. Deschner, B. Lothenbach, F. Winnefeld, J. Neubauer, Effect of temperature on the
- 681 hydration of Portland cement blended with siliceous fly ash, Cement Concrete Res 52 (2013)
- 682 169-181.
- [43] T. Matschei, B. Lothenbach, F.P. Glasser, Thermodynamic properties of Portland cement
- 684 hydrates in the system CaO-Al2O3-SiO2-CaSO4-CaCO3-H2O, Cement Concrete Res
- 685 37(10) (2007) 1379-1410.
- 686 [44] D. Glosser, P. Suraneni, O.B. Isgor, W.J. Weiss, Estimating reaction kinetics of
- cementitious pastes containing fly ash, Cement and Concrete Composites (2020) 103655.
- 688 [45] D.B. Glosser, Equilibrium and Non-equilibrium Thermodynamic Modeling of Cement
- Pastes Containing Supplementary Cementitious Materials, Civil Engineering, Oregon State
- 690 University, Corvallis OR, 2020.
- 691 [46] P. Suraneni, V.J. Azad, B.O. Isgor, W.J. Weiss, Calcium oxychloride formation in pastes
- 692 containing supplementary cementitious materials: Thoughts on the role of cement and
- supplementary cementitious materials reactivity, RILEM Technical Letters 1 (2016) 24-30.
- 694 [47] O.M. Jensen, P.F. Hansen, Water-entrained cement-based materials I. Principles and
- theoretical background, Cement Concrete Res 31(4) (2001) 647-654.
- 696 [48] P. Ghods, O. Isgor, G. McRae, T. Miller, The effect of concrete pore solution composition
- on the quality of passive oxide films on black steel reinforcement, Cement and Concrete
- 698 Composites 31(1) (2009) 2-11.

- 699 [49] X. Hou, L.J. Struble, R.J. Kirkpatrick, Formation of ASR gel and the roles of CSH and
- 700 portlandite, Cement Concrete Res 34(9) (2004) 1683-1696.
- 701 [50] T. Matschei, F.P. Glasser, Temperature dependence, 0 to 40 degrees C, of the mineralogy
- of Portland cement paste in the presence of calcium carbonate, Cement Concrete Res 40(5)
- 703 (2010) 763-777.
- 704 [51] J. Monical, E. Unal, T. Barrett, Y. Farnam, W.J. Weiss, Reducing joint damage in concrete
- 705 pavements: Quantifying calcium oxychloride formation, Transportation Research Record
- 706 2577(1) (2016) 17-24.
- 707 [52] P. Suraneni, N. Salgado, H. Carolan, C. Li, V. Azad, B. Isgor, J. Ideker, J. Weiss,
- 708 Mitigation of deicer damage in concrete pavements caused by calcium oxychloride formation—
- use of ground lightweight aggregates, International RILEM Conference on Materials, Systems
- and Structures in Civil Engineering, Lyngby, Denmark, 2016, pp. 171-180.
- 711 [53] P. Suraneni, J. Monical, E. Unal, Y. Farnam, J. Weiss, Calcium oxychloride formation
- 712 potential in cementitious pastes exposed to blends of deicing salt, ACI Mater. J 114(4) (2017)
- 713 631-641.
- 714 [54] S.N. Whatley, P. Suraneni, V.J. Azad, O.B. Isgor, J. Weiss, Mitigation of calcium
- oxychloride formation in cement pastes using undensified silica fume, J Mater Civil Eng 29(10)
- 716 (2017) 04017198.
- 717 [55] B. Pichler, C. Hellmich, J. Eberhardsteiner, J. Wasserbauer, P. Termkhajornkit, R.
- Barbarulo, G. Chanvillard, Effect of gel-space ratio and microstructure on strength of hydrating
- 719 cementitious materials: An engineering micromechanics approach, Cement Concrete Res 45
- 720 (2013) 55-68.
- 721 [56] M.T. Hasholt, M.H.S. Jespersen, O.M. Jensen, Mechanical properties of concrete with
- SAP part I: Development of compressive strength, International RILEM conference on use of

- superabsorbent polymers and other new additives in concrete, RILEM Publications SARL,
- 724 2010, p. 10.
- 725 [57] A. Princigallo, P. Lura, K. van Breugel, G. Levita, Early development of properties in a
- cement paste: A numerical and experimental study, Cement Concrete Res 33(7) (2003) 1013-
- 727 1020.
- 728 [58] E.K. Nambiar, K. Ramamurthy, Models for strength prediction of foam concrete,
- 729 Materials and structures 41(2) (2008) 247.
- 730 [59] C. Ouyang, A damage model for sulfate attack of cement mortars, Cement, concrete and
- 731 aggregates 11(2) (1989) 92-99.
- 732 [60] G.E. Archie, The electrical resistivity log as an aid in determining some reservoir
- characteristics, Transactions of the AIME 146(01) (1942) 54-62.
- 734 [61] W.J. Weiss, T.J. Barrett, C. Qiao, H. Todak, Toward a specification for transport
- properties of concrete based on the formation factor of a sealed specimen, Advances in Civil
- 736 Engineering Materials 5(1) (2016) 179-194.
- 737 [62] M.K. Moradllo, C. Qiao, B. Isgor, S. Reese, W.J. Weiss, Relating formation factor of
- concrete to water absorption, ACI Mater J. https://doi. org/10.14359/51706844 (2018).
- 739 [63] W.J. Weiss, R.P. Spragg, O.B. Isgor, M.T. Ley, T. Van Dam, Toward performance
- 740 specifications for concrete: linking resistivity, RCPT and diffusion predictions using the
- 741 formation factor for use in specifications, High tech concrete: Where technology and
- engineering meet, Springer2018, pp. 2057-2065.
- 743 [64] O.B. Isgor, J. Weiss, A nearly self-sufficient framework for modelling reactive-transport
- processes in concrete, Materials and Structures 52(1) (2019).
- 745 [65] K.A. Snyder, The relationship between the formation factor and the diffusion coefficient
- of porous materials saturated with concentrated electrolytes: theoretical and experimental
- 747 considerations, (2000).

- 748 [66] C. Qiao, M.K. Moradllo, H. Hall, M.T. Ley, J. Weiss, Electrical Resistivity and Formation
- 749 Factor of Air-Entrained Concrete, ACI Materials Journal 116(3) (2019).
- 750 [67] M.K. Moradllo, C. Qiao, H. Hall, M.T. Ley, S.R. Reese, J. Weiss, Quantifying Fluid
- 751 Filling of the Air Voids in Air Entrained Concrete Using Neutron Radiography, Cement and
- 752 Concrete Composites In Press (2019).
- 753 [68] M.K. Moradllo, C. Qiao, M. Keys, H. Hall, M.T. Lay, S.R. Reese, J. Weiss, Quantifying
- 754 Fluid Absorption in Air-Entrained Concrete Using Neutron Radiography, ACI Materials
- 755 Journal In Press (2019).
- 756 [69] J. Weiss, M.T. Ley, O.B. Isgor, T. Van Dam, Toward performance specifications for
- 757 concrete durability: using the formation factor for corrosion and critical saturation for freeze-
- 758 thaw, Proceedings of the 96th Annual Transportation Research Board, Washington, DC, USA
- 759 (2017) 8-12.
- 760 [70] E.J. Garboczi, D.P. Bentz, Computer simulation of the diffusivity of cement-based
- materials, Journal of materials science 27(8) (1992) 2083-2092.
- 762 [71] B.J. Christensen, T. Coverdale, R.A. Olson, S.J. Ford, E.J. Garboczi, H.M. Jennings, T.O.
- 763 Mason, Impedance spectroscopy of hydrating cement-based materials: measurement,
- interpretation, and application, Journal of the American Ceramic Society 77(11) (1994) 2789-
- 765 2804.
- 766 [72] J. Zhang, Z.J. Li, Application of GEM Equation in Microstructure Characterization of
- 767 Cement-Based Materials, J Mater Civil Eng 21(11) (2009) 648-656.
- 768 [73] A. Koponen, M. Kataja, J. Timonen, Permeability and effective porosity of porous media,
- 769 Phys Rev E 56(3) (1997) 3319-3325.
- 770 [74] H.Y. Ma, D.S. Hou, Z.J. Li, Two-scale modeling of transport properties of cement paste:
- 771 Formation factor, electrical conductivity and chloride diffusivity, Comp Mater Sci 110 (2015)
- 772 270-280.

- 773 [75] B. Isgor, J. Ideker, D. Trejo, J. Weiss, K. Bharadwaj, A. Choudhary, C.K.S. Teja, D.
- Glosser, G. Vasudevan, Development of a performance-based mixture proportioning procedure
- for concrete incorporating off-spec fly ash, Final Report, Energy Power Research Institute
- 776 (EPRI); Oregon State University, 2020.
- 777 [76] R.M. Ghantous, J.W. Weiss, Does the Water to Cement Ratio of Concrete Impact the
- 778 Value of its Critical Degree of Saturation?, 10th International Conference on Fracture
- 779 Mechanics of Concrete and Concrete Structures, Bayonne (France), 2019.
- 780 [77] N.T. Todd, Assessing risk reduction of high early strength concrete mixtures, Purdue
- 781 University, 2015.
- 782 [78] T. Kim, J. Olek, Effects of sample preparation and interpretation of thermogravimetric
- curves on calcium hydroxide in hydrated pastes and mortars, Transportation research record
- 784 2290(1) (2012) 10-18.
- 785 [79] AASHTO, Standard Method of Test for Determining the Total Pore Volume in Hardened
- 786 Concrete Using Vacuum Saturation, AASHTO TP 135-20, American Association of State
- 787 Highway and Transportation Officials, Washington DC, 2020.
- 788 [80] A.A.o.S.H.a.T. Officials, Standard Method of Test for Electrical Resistivity of a Concrete
- 789 Cylinder Tested in a Uniaxial Resistance Test, TP 119-20, AASHTO, Washington DC, 2020.
- 790 [81] R. Spragg, C. Villani, K. Snyder, D. Bentz, J.W. Bullard, J. Weiss, Factors That Influence
- 791 Electrical Resistivity Measurements in Cementitious Systems, Transportation Research Record
- 792 (2342) (2013) 90-98.
- 793 [82] A.T. Coyle, R.P. Spragg, P. Suraneni, A.N. Amirkhanian, W.J. Weiss, Comparison of
- 794 linear temperature corrections and activation energy temperature corrections for electrical
- resistivity measurements of concrete, Advances in Civil Engineering Materials 7(1) (2018)
- 796 174-187.

- 797 [83] R. Spragg, C. Qiao, T. Barrett, J. Weiss, Assessing a concrete's resistance to chloride ion
- 798 ingress using the formation factor, Corrosion of steel in concrete structures, Elsevier2016, pp.
- 799 211-238.
- 800 [84] B. Lothenbach, A. Nonat, Calcium silicate hydrates: solid and liquid phase composition,
- 801 Cement Concrete Res 78 (2015) 57-70.
- 802 [85] B. Marsh, R. Day, D. Bonnery, Strength gain and calcium hydroxide depletion in hardened
- cement pastes containing fly ash, Magazine of Concrete Research 38(134) (1986) 23-29.
- 804 [86] B.K. Marsh, R.L. Day, Pozzolanic and Cementitious Reactions of Fly-Ash in Blended
- 805 Cement Pastes, Cement Concrete Res 18(2) (1988) 301-310.
- 806 [87] M. Radlinski, J. Olek, Investigation into the synergistic effects in ternary cementitious
- systems containing portland cement, fly ash and silica fume, Cement and Concrete Composites
- 808 34(4) (2012) 451-459.
- 809 [88] R.M. Ghantous, Y. Farnam, E. Unal, J. Weiss, The influence of carbonation on the
- formation of calcium oxychloride, Cement and Concrete Composites 73 (2016) 185-191.
- 811 [89] P. Chindaprasirt, C. Jaturapitakkul, T. Sinsiri, Effect of fly ash fineness on compressive
- strength and pore size of blended cement paste, Cement Concrete Comp 27(4) (2005) 425-428.
- [90] M. Khan, C. Lynsdale, P. Waldron, Porosity and strength of PFA/SF/OPC ternary blended
- 814 paste, Cement Concrete Res 30(8) (2000) 1225-1229.
- 815 [91] S. Pandey, R. Sharma, The influence of mineral additives on the strength and porosity of
- 816 OPC mortar, Cement Concrete Res 30(1) (2000) 19-23.
- [92] M. Thomas, Supplementary cementing materials in concrete, CRC press2013.
- 818 [93] B. Pichler, C. Hellmich, Upscaling quasi-brittle strength of cement paste and mortar: A
- multi-scale engineering mechanics model, Cement Concrete Res 41(5) (2011) 467-476.
- 820 [94] B. Pichler, C. Hellmich, J. Eberhardsteiner, J. Wasserbauer, P. Termkhajornkit, R.
- 821 Barbarulo, G. Chanvillard, The Counteracting Effects of Capillary Porosity and of Unhydrated

- 822 Clinker Grains on the Macroscopic Strength of Hydrating Cement Paste–A Multiscale Model,
- Mechanics and Physics of Creep, Shrinkage, and Durability of Concrete: A Tribute to Zdeňk
- 824 P. Bažant2013, pp. 40-47.
- 825 [95] R.D. Hooton, Permeability and pore structure of cement pastes containing fly ash, slag,
- and silica fume, Blended cements, ASTM International 1986.
- 827 [96] V.G. Papadakis, E.J. Pedersen, H. Lindgreen, An AFM-SEM investigation of the effect of
- silica fume and fly ash on cement paste microstructure, Journal of Materials Science 34(4)
- 829 (1999) 683-690.
- [97] P.T. Durdziński, M.B. Haha, S.A. Bernal, N. De Belie, E. Gruyaert, B. Lothenbach, E.M.
- Méndez, J.L. Provis, A. Schöler, C. Stabler, Outcomes of the RILEM round robin on degree of
- reaction of slag and fly ash in blended cements, Materials and Structures 50(2) (2017) 135.
- 833 [98] F. Deschner, B. Münch, F. Winnefeld, B. Lothenbach, Quantification of fly ash in
- hydrated, blended Portland cement pastes by backscattered electron imaging, Journal of
- 835 microscopy 251(2) (2013) 188-204.
- 836 [99] X. Feng, E.J. Garboczi, D.P. Bentz, P.E. Stutzman, T.O. Mason, Estimation of the degree
- of hydration of blended cement pastes by a scanning electron microscope point-counting
- 838 procedure, Cement Concrete Res 34(10) (2004) 1787-1793.
- 839 [100] M. Narmluk, T. Nawa, Effect of curing temperature on pozzolanic reaction of fly ash in
- blended cement paste, International Journal of Chemical Engineering and Applications 5(1)
- 841 (2014) 31.
- [101] S.H. Kosmatka, B. Kerkhoff, W.C. Panarese, Design and control of concrete mixtures,
- 843 Portland Cement Association Skokie, IL2002.